Robotica (2002) volume 20, pp. 341–352. © 2002 Cambridge University Press
DOI: 10.1017/S0263574702004058 Printed in the United Kingdom

Compensation of geometric and elastic errors in large manipulators with an application to a high accuracy medical system

Ph. Drouet*, S. Dubowsky**, S. Zeghloul* and C. Mavroidis†

(Received in Final Form: December 12, 2001)

SUMMARY
A method is presented that compensates for manipulator end-point errors in order to achieve very high position accuracy. The measured end-point error is decomposed into generalized geometric and elastic error parameters that are used in an analytical model to calibrate the system as a function of its configuration and the task loads, including any payload weight. The method exploits the fundamental mechanics of serial manipulators to yield a non-iterative compensation process that only requires the identification of parameters that are function only of one variable. The resulting method is computationally simple and requires far less measured data that might be expected. The method is applied to a six degrees-of-freedom (DOF) medical robot that positions patients for cancer proton therapy to enable it to achieve very high accuracy. Experimental results show the effectiveness of the method.

KEYWORDS: Errors; Compensation; Large manipulators; Medical system; Accuracy.

1. INTRODUCTION

Many tasks require very high accuracy positioning large manipulators. For example, a key element of a new cancer research and treatment facility, at the Massachusetts General Hospital (MGH), is a robotic patient positioning system (PPS).[1] To meet the medical requirements, the PPS must position a patient under a proton radiation beam during cancer therapy with very good accuracy. The permitted end-point position error must be less than ± 0.5 mm.[2] These requirements also mandate a manipulator with a large workspace (a diameter of almost 6 meters), a cantilevered design, and a large range of payloads (patient weights vary from 20 Kg to 200 Kg). The result is a system with inherently low accuracy.[3] Analysis and experiments show that the end-point errors of the system are in the range of 7 to 8 mm,[4] far larger than the specification of ± 0.5 mm. The source of these errors include small geometric distortions in the system due to manufacturing tolerances, thermal effects, wear, and joint transducer errors. The largest source of error is the elastic deformation of the system's components under its own weight and the weight of the patient.[5]

Reducing the error by changing the physical design of the PPS was not technically or economically practical. Furthermore, the effective end-point is the site of the tumor inside the body, which is subjected to very high radiation levels, and no sensor can measure its position in real time in safe conditions for the patient. Error compensation using conventional end-point feedback is then not feasible. Hence, the objective of this study was to develop a method that would permit the end-point error to be reduced at least by an order of magnitude using a openloop compensation.

Considerable research has been performed to improve the accuracy of manipulators using model based calibration methods.[6] In their simplest form, calibration procedures consists of developing a system error model, making series of off-line measurements of manipulators' errors, and using these measurements to identify the parameters of the error model. The model is then used to predict and compensate for any errors during the manipulator's operation. Error models based on screw theory, homogeneous matrices, Denavit and Hartenberg coordinates, and Jacobian matrices have been developed.[7–9] Later methods have been proposed, such as those based on complete and parametrically continuous (CPC) models have been proposed to improve the effectiveness of manipulator calibration.[10] These calibration approaches assume that the errors in the system are dominated by geometric errors in the system kinematic structure, due to such factors as manufacturing tolerance errors.[11–13] The methods are very effective for many applications where the elastic deformations, due to task and gravitational loading, are small. In these cases, the errors of the system will be only a function of the configuration of the manipulator. In a general six DOF serial manipulator, it is required to make end-point error measurements as a function of the six joint variables of the manipulator to perform the calibration. Calibrating the entire workspace of a six DOF manipulator may take many thousands of measurements which can be very time consuming and costly. Research has focused on improved sensing techniques and equipment for calibration, such as mobile camera systems and laser tracking systems.[14–16] Methods have been developed to the optimization of measurement configurations during calibration.[17,18] Other work has suggested local calibration that in some cases would improve the effectiveness of the kinematic calibration problem.[19] Nonetheless, the problem of the number of measurements required to calibrate a general serial manipulator has

* Laboratoire de Mécanique des Solides, Université de Poitiers, 86960 Futuroscope (FRANCE):
E-mail: said@lms.univ-poitiers.fr
** Massachusetts Institute of Technology, Department of Mechanical Engineering, Cambridge, MA (USA).
† Department of Mechanical and Aerospace Engineering, Rutgers University, Piscataway, NJ (USA).

remained a serious practical problem, even when elastic effects are neglected. For the PPS, the measurements could take several days and cost thousands of dollars, even with the most modern automated theodolites measurement systems.

The question of modeling of elastic effects in manipulators has been considered by researchers for many years.[20] Calibration methods to compensate for static elastic effects in manipulators have yet to be developed, except for a few simple special cases.[21] Clearly, calibration for dynamic elastic effects is a very difficult problem. To the best of our knowledge, research to develop practical calibration methods for the general problem of calibration compensation of combined geometric and elastic static deformations, such as found in the PPS, has yet to be addressed. While in theory the solution to this problem should not be fundamentally more difficult than the classical kinematic calibration problem. However, it does present a serious additional problem if elastic effects due to task loads are included. As a matter of fact, as discussed above, in the kinematic error calibration problem, the end-point errors of a nonredundant manipulator is mapped as a function of the manipulator's six-dimensional configuration vector, which may already be a problem of a significant size. Taking in account the elastic effects as new dimensions for the mapping would expand too dramatically the size of the problem.

If the task load is a six-axis wrench (three forces and three moments), such as in the PPS, the end-point error will be a function of the 12 variables, the six joint parameters and the six task wrench variables. A simple analysis shows, with a straightforward calibration with elastic effects, that it requires an order of 10^6 times as many experimental measurements in comparison to basic kinematic calibration. The amount of time spent on making such a large number of measurements would not be technically and economically feasible.

In this paper, the problem of compensating for combined geometric and elastic errors is addressed by studying the fundamental mechanics of the system. An error model of a serial-link manipulator model is developed in which the end-point error is explicitly expressed in terms of generalized geometric and elastic errors. These generalized errors are functions of the joint variables and loads applied to the system. It is shown that it is possible to represent the system's generalized errors by parameters that are functions only of a single variable. The parameters are identified from off-line experimental data and are then used to compensate for errors during system operation. The fact that the parameters are a function only of a single variable is shown to greatly reduce the number of measurements required, leading to a practical compensation method for realistic applications.

The method was applied to the PPS at the Massachusetts General Hospital of Harvard University. First experimental results showed that the initial PPS end-point accuracy is approximately ± 7.0 mm, compared to the requirement of ± 0.5 mm. By applying the method, the errors were reduced to ± 0.4 mm, which represents a reduction factor of about 20. Only approximately 300 measurements were required to identify all the parameters of the model needed to calibrate the system over its entire workspace and for patients weighing between 20 and 200 Kg. These results clearly indicate the effectiveness and practicality of the method that is now being used at MGH.

2. ANALYTICAL DEVELOPMENT

2.1. Geometric and elastic error model

The end-point error model is developed using generalized errors.[4] Assuming that the error sources are small, a linearized model is developed for simplicity. The generalized errors are then decomposed into geometric and elastic errors. It is shown that the generalized errors can be represented by parameters that are functions only of a single variable.

Consider the n d.o.f serial manipulator (shown in Figure 1) with $n+1$ links and where an inertial frame, F_I, is centered at O_I. The points O_0 to O_{n-1} are located at to each manipulator joint. The point O_T defines the manipulator end-point. A reference frame F_i is fixed to the i^{th} link at O_i.

The classical 4×4 homogeneous matrix transformation from frame F_{i-1} to frame F_i is given by:[22]

$$\mathbf{A_i}=\begin{pmatrix}\mathbf{R_i} & \mathbf{T_i}\\ 0 & 1\end{pmatrix} \tag{1}$$

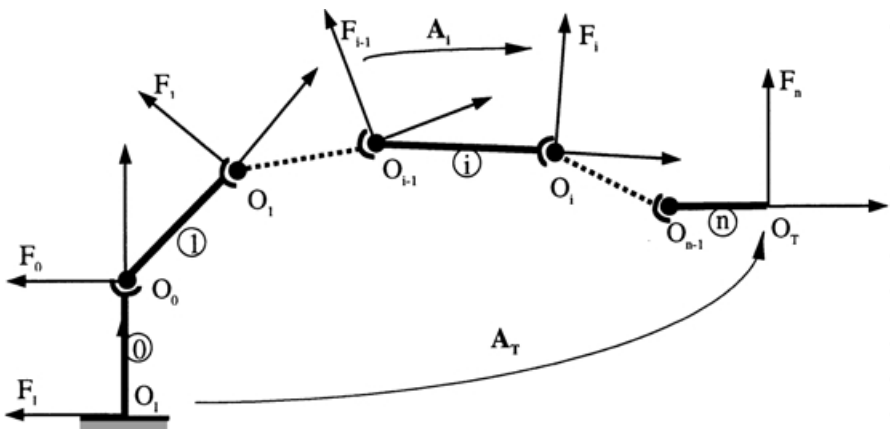

Fig. 1. Coordinate frames for an ideal n DOF manipulator.

https://doi.org/10.1017/S0263574702004058 Published online by Cambridge University Press

where $\mathbf{R_i}$ is the 3×3 matrix representing the orientation of F_i with respect to F_{i-1}, and $\mathbf{T_i}$ is composed of components of the vector $O_{i-1}O_i$ expressed in the frame F_{i-1}. The elements of $\mathbf{A_i}$ depend on the geometry of the manipulators links, represented by a structure vector $\mathbf{s_i}$ and on its joint variable, q_i. The configuration vector $\mathbf{q}$ is formed by the joints variables q_i ($i=1, \ldots, n$).

In the following notations, a superscript "i" indicates the ideal of the end-point position (without any errors), A superscript "r" indicates the real position (with errors). The end-point frame F_n position and orientation coordinates, with respect to the inertial frame, form a 6×1 vector, $\mathbf{X_T}^i$. Where $\mathbf{X_T}^i$ is a nonlinear function of the system geometric parameters and joints variables, respectively $\mathbf{s}$ and $\mathbf{q}$:

$$\mathbf{X_T}^i=[t_x\ t_y\ t_z\ \theta_x\ \theta_y\ \theta_z]^T=\mathbf{f}^i(\mathbf{s},\mathbf{q}) \tag{2}$$

$\mathbf{X_T}^i$ can be obtained from the well known loop closure equation:[22]

$$\mathbf{A_T}^i=\mathbf{A_0}\,\mathbf{A_1}\ldots\mathbf{A_n} \tag{3}$$

Equation (3) can be written as:

$$\mathbf{A_T}^i=\left[\begin{array}{ccc|c} r_{11} & r_{12} & r_{13} & t_x \\ r_{21} & r_{22} & r_{23} & t_y \\ r_{31} & r_{32} & r_{33} & t_z \\ \hline 0 & 0 & 0 & 1 \end{array}\right]$$

$$=\left[\begin{array}{ccc|c} c\theta_y\,c\theta_z & s\theta_x\,s\theta_y\,c\theta_z-s\theta_z\,c\theta_x & c\theta_z\,s\theta_y\,c\theta_x+s\theta_z\,s\theta_x & t_x \\ s\theta_z\,c\theta_y & c\theta_x\,c\theta_z & s\theta_x\,s\theta_y\,c\theta_x-s\theta_x\,c\theta_z & t_y \\ -s\theta_y & s\theta_x\,c\theta_y & c\theta_x\,c\theta_y & t_z \\ \hline 0 & 0 & 0 & 1 \end{array}\right] \tag{4}$$

The first three components of $\mathbf{X_T}^i$ are obtained directly from Equation (4). The 3 variables ($\theta_x\ \theta_y\ \theta_z$) of $\mathbf{X_T}^i$, corresponding to 3 successive rotations around Z, Y and X, are obtained from Equation (4) by algebraic manipulations.

The errors in the geometry of a manipulator result in a slight displacement of the frames, located at the manipulator's joints, from their ideal locations. The displacement between the i^{th} real and the ideal frame locations, see Figure 2, can be represented by six parameters, $\varepsilon_{1,i}$ to $\varepsilon_{6,i}$. These six parameters represent the effect of all the local errors (machining, mounting elastic deformations, . . .) on the frame location of the F_i. The parameters $\varepsilon_{1,i}$, $\varepsilon_{2,i}$ and $\varepsilon_{3,i}$, are the three displacement coordinates of the vector from F_i^r and F_i^i. The parameters $\varepsilon_{4,i}$, $\varepsilon_{5,i}$ and $\varepsilon_{6,i}$ are the three angles defining the orientation of F_i^r with respect to F_i^i.

A 4×4 homogeneous matrix, $\mathbf{E_i}$, representing this error distortion can be defined on a "link by link" basis.[3,4] Matrix $\mathbf{E_i}$ is written as follow:

$\mathbf{E_i}=$

$$\left[\begin{array}{cccc} c\varepsilon_{6,i}\,c\varepsilon_{5,i} & s\varepsilon_{4,i}\,s\varepsilon_{5,i}\,c\varepsilon_{6,i}-s\varepsilon_{6,i}\,c\varepsilon_{4,i} & c\varepsilon_{6,i}\,s\varepsilon_{5,i}\,c\varepsilon_{4,i}+s\varepsilon_{6,i}\,s\varepsilon_{4,i} & \varepsilon_{1,i} \\ s\varepsilon_{6,i}\,c\varepsilon_{5,i} & c\varepsilon_{4,i}\,c\varepsilon_{6,i}+s\varepsilon_{4,i}\,s\varepsilon_{5,i}\,s\varepsilon_{6,i} & s\varepsilon_{6,i}\,s\varepsilon_{5,i}\,c\varepsilon_{4,i}-s\varepsilon_{4,i}c\varepsilon_{6,i} & \varepsilon_{2,i} \\ -s\varepsilon_{5,i} & s\varepsilon_{4,i}\,c\varepsilon_{5,i} & c\varepsilon_{4,i}\,c\varepsilon_{5,i} & \varepsilon_{3,i} \\ 0 & 0 & 0 & 1 \end{array}\right]$$

The parameters $\varepsilon_{j,i}$ are called "generalized errors". For an n DOF manipulator, there are $6\times(n+1)$ generalized errors parameters:

$$\boldsymbol{\varepsilon}=[\varepsilon_{1,0},\ \varepsilon_{2,0},\ \ldots,\ \varepsilon_{6,0},\ \ldots,\ \varepsilon_{1,n},\ \ldots,\ \varepsilon_{6,n}]$$

The manipulator loop closure equation, including errors, becomes:

$$\mathbf{A_T}^r=\mathbf{A_T}^i\mathbf{E_T}=\mathbf{A_0}\,\mathbf{E_0}\,\mathbf{A_1}\,\mathbf{E_1}\ldots\mathbf{A_n}\,\mathbf{E_n} \tag{5}$$

As with Equation (3), the end-point coordinates vector $\mathbf{X_T}^r$ can be determined as a function of $\mathbf{s}$, $\mathbf{q}$, and $\boldsymbol{\varepsilon}$ from Equation (5):

$$\mathbf{X_T}^r=\mathbf{f}^r(\mathbf{s},\mathbf{q},\boldsymbol{\varepsilon}) \tag{6}$$

2.2. A linear generalized error model

Assuming that errors (ε) are small, the matrix $\mathbf{E_i}$ can be written as:

$$\mathbf{E_i}=\left(\begin{array}{cccc} 1 & -\varepsilon_{6,i} & \varepsilon_{5,i} & \varepsilon_{1,i} \\ \varepsilon_{6,i} & 1 & -\varepsilon_{4,i} & \varepsilon_{2,i} \\ -\varepsilon_{5,i} & \varepsilon_{4,i} & 1 & \varepsilon_{3,i} \\ 0 & 0 & 0 & 1 \end{array}\right) \tag{7}$$

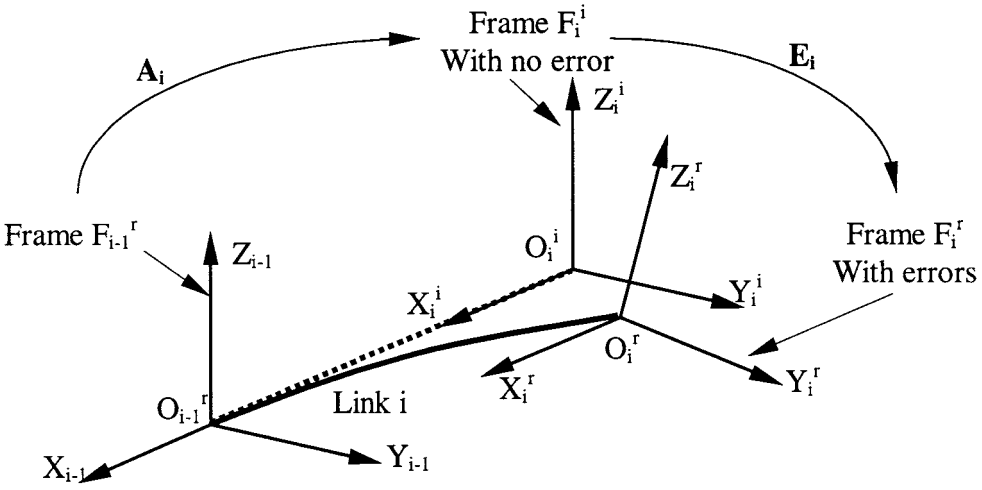

Fig. 2. Displacement from frame F_{i-1}^r to F_i^r.

https://doi.org/10.1017/S0263574702004058 Published online by Cambridge University Press

Equation (7) is then separated in its error part and non error part: $\mathbf{E_i}=\mathbf{E_{ri}}+\mathbf{I}$, where $\mathbf{I}$ is the identity matrix. We also define $\mathbf{E_{rT}}$ as follows:

$$\mathbf{E_{rT}}=\begin{pmatrix} 0 & -\Delta X_6 & \Delta X_5 & \Delta X_1 \\ \Delta X_6 & 0 & -\Delta X_4 & \Delta X_2 \\ -\Delta X_5 & \Delta X_4 & 0 & \Delta X_3 \\ 0 & 0 & 0 & 0 \end{pmatrix}=\mathbf{E_T}-\mathbf{I} \quad (8)$$

Combining Equation (5), Equation (7) and Equation (8) and eliminating second order and higher terms yields the following linearized loop closure equation:

$$\mathbf{A_0E_{r0}A_1A_2}\ldots\mathbf{A_n}+\mathbf{A_n}\ldots\mathbf{A_1E_{r1}A_{i+1}}\ldots\mathbf{A_n}+\ldots$$
$$+\mathbf{A_0A_1}\ldots\mathbf{A_nE_{rn}}=\mathbf{A_T}^{r}-\mathbf{A_T}^{I}=\mathbf{A_T}^{i}\mathbf{E_{rT}} \quad (9)$$

For a non-redundant manipulator, in a non-singular configuration, Equation (9) can be multiplied by the inverse of $\mathbf{A_T}^{i}$ so that an expression for $\mathbf{E_T}^{r}$ in frame F_n is obtained:

$$\mathbf{E_{rT}}=(\mathbf{A_1A_2}\ldots\mathbf{A_n})^{-1}\mathbf{E_{r0}}(\mathbf{A_1A_2}\ldots\mathbf{A_n})$$
$$+(\mathbf{A_{i+1}}\ldots\mathbf{A_n})^{-1}\mathbf{E_{ri}}(\mathbf{A_{i+1}}\ldots\mathbf{A_n})+\ldots+\mathbf{E_{rn}} \quad (10)$$

Thus the six matrix $\mathbf{E_{rT}}$ elements can be readily identified. Each is a linear function of the generalized errors. The six coordinates of the end effector error vector $\Delta\mathbf{X}$ can be now obtained from Equation (10) using the linearized form of $\mathbf{E_{rT}}$:

$$\Delta\mathbf{X}=\mathbf{g}(\mathbf{q},\boldsymbol{\varepsilon},\mathbf{s}) \quad (11)$$

The matrix form of Equation (11) is given by a generalized errors jacobian:

$$\Delta\mathbf{X}=\mathbf{J}(\mathbf{q},\mathbf{s})\boldsymbol{\varepsilon} \quad (12)$$

where $\mathbf{J}=\partial\mathbf{f}^{r}/\partial\boldsymbol{\varepsilon}$ is a 6 by (6n+6) matrix which can be obtained in an explicit algebraic form using symbolic manipulation software such as Maple.

The symbol $\mathbf{s}$ is dropped from the notation to simplify the expressions.

2.3. Geometric and elastic errors, compliance parameters

The generalized errors are separated into geometric errors and elastic errors:

$$\boldsymbol{\varepsilon}(\mathbf{q},\mathbf{W})=\boldsymbol{\varepsilon}_g(\mathbf{q})+\boldsymbol{\varepsilon}_e(\mathbf{q},\mathbf{W}) \quad (13)$$

where $\boldsymbol{\varepsilon}_e=[\boldsymbol{\varepsilon}_{e0},\boldsymbol{\varepsilon}_{e1},\ldots,\boldsymbol{\varepsilon}_{en}]$ is the elastic errors vector and $\boldsymbol{\varepsilon}_g=[\boldsymbol{\varepsilon}_{g0},\boldsymbol{\varepsilon}_{g1},\ldots,\boldsymbol{\varepsilon}_{gn}]$ is the geometric errors vector. $\boldsymbol{\varepsilon}_{gi}$ and $\boldsymbol{\varepsilon}_{ei}$ are 6×1 vectors, $\mathbf{W}$ is the set of all the external wrenches applied to the manipulator. Note that while the elastic errors are function of $\mathbf{q}$ and $\mathbf{W}$, the geometric errors are function only of $\mathbf{q}$. Equation (12) becomes:

$$\Delta\mathbf{X}=\mathbf{J}(\mathbf{q})\boldsymbol{\varepsilon}_g(\mathbf{q})+\mathbf{J}(\mathbf{q})\boldsymbol{\varepsilon}_e(\mathbf{q},\mathbf{W})=\Delta\mathbf{X_g}+\Delta\mathbf{X_e} \quad (14)$$

Where $\Delta\mathbf{X_e}$ is the end effector error due to elastic deformations only and $\Delta\mathbf{X_g}$ the end effector errors due to geometric errors only.

Equation (14) can be simplified by first noting that, for a manipulator with an open tree configuration, such as a serial manipulator, each joint motion is independent of the others. Therefore, the geometric errors $\boldsymbol{\varepsilon}_{gi}$ of link i are function only of the joint variable q_i.

Also, assuming that quasi-static conditions prevail, the wrench at each link can be obtained by simple static analysis. Further, for a quasi-static serial manipulator, the wrench $\mathbf{W_{i,i}}$, applied to the end of link i at O_i with respect to the frame F_i, is only a function of the joint variables following q_i, that is to say $q_{i+1}, q_{i+2}, \ldots, q_n$, and of the loads applied on links i+l, . . . , link n, such as the load applied at the end effector.

Finally, since errors are considered to be small, we can assume that the elastic deformations of the i^{th} link are linear with $\mathbf{W}$, which leads to:

$$\boldsymbol{\varepsilon}_{ei}=\mathbf{C_i}(q_i)\mathbf{W_{i,i}}([q_{i+1},\ldots.q_n],\mathbf{W}) \quad (15)$$

where $\mathbf{C_i}$ is a 6×6 symmetrical compliance matrix for the link i[23] composed by 21 independent elements. The matrix $\mathbf{C_i}$ is function of the geometry of the link. For rotary joints, the geometry of a link does not change, so that $\mathbf{C_i}$ is constant. For prismatic joints, the length of the i^{th} link changes with q_i, so the elements c_{ijk} of $\mathbf{C_i}$, called compliance parameters, are only function of q_i.

Since $\boldsymbol{\varepsilon}_{ei}$ is linear with respect to the compliance parameters and $\Delta\mathbf{X_e}$ is linear with $\boldsymbol{\varepsilon}_{ei}$, $\Delta\mathbf{X_e}$ is linear with respect to the compliance parameters too. The elastic error vector $\Delta\mathbf{X_e}$ can be written as follows:

$$\Delta\mathbf{X_e}=\mathbf{J}[\ldots,\mathbf{C_i},\ldots][\ldots,\mathbf{W_{i,i}},\ldots]^{T}=\mathbf{M_e}(\mathbf{q},\mathbf{W})\mathbf{c} \quad (16)$$

where $\mathbf{c}$ is a vector formed from the 21 elements of $\mathbf{C_i}$ (i=0, . . . , 6), $\mathbf{c}=[\mathbf{c_0},\mathbf{c_1}(q_1),\ldots,\mathbf{c_n}(q_n)]$, and $\mathbf{M_e}$ is the end effector errors jacobian with respect to the compliance parameters: $\mathbf{M_e}=\partial\Delta\mathbf{X_e}/\partial\mathbf{c}$. The matrix $\mathbf{M_e}$ can be obtained in explicit symbolic form by using, for instance, the software Maple V.

Finally, combining Equation (14) and Equation (16) gives the geometric and elastic errors model at the manipulator end-point:

$$\Delta\mathbf{X}=\Delta\mathbf{X_g}+\Delta\mathbf{X_e}=\mathbf{J}(\mathbf{q})\boldsymbol{\varepsilon}_g+\mathbf{M_e}(\mathbf{q},\mathbf{W})\mathbf{c} \quad (17)$$

Since

$$\boldsymbol{\varepsilon}_g=[\boldsymbol{\varepsilon}_{g0},\boldsymbol{\varepsilon}_{g1}(q_1),\ldots,\boldsymbol{\varepsilon}_{gn}(q_n)]$$

and

$$\mathbf{c}=[\mathbf{c_0},\mathbf{c_1}(q_1),\ldots,\mathbf{c_n}(q_n)],$$

the end effector errors can be expressed with parameters that are only functions of one variable.

With this model, the prediction of the end-point errors is obtained by previously identifying $\boldsymbol{\varepsilon}_g$ and $\mathbf{c}$ vectors from experimental data. The vector $\boldsymbol{\varepsilon}_g$ is a $6\times n$ vector and $\mathbf{c}$ is a $21\times(n+1)$ vector. Note that the number of vector $\mathbf{c}$ terms will be significantly reduced in most of the cases. Some simple knowledge on the system's physics such as symmetries in links geometry can be used to simplify the form of the compliance matrices.

Assuming that the parameters of the model are identified, the geometric and elastic errors model can be used for end-point errors compensation, following the process described by the algorithm in Figure 3.

When the corrected joint variables are input as command on the considered manipulator, the desired position is reached with very small remaining error.

https://doi.org/10.1017/S0263574702004058 Published online by Cambridge University Press

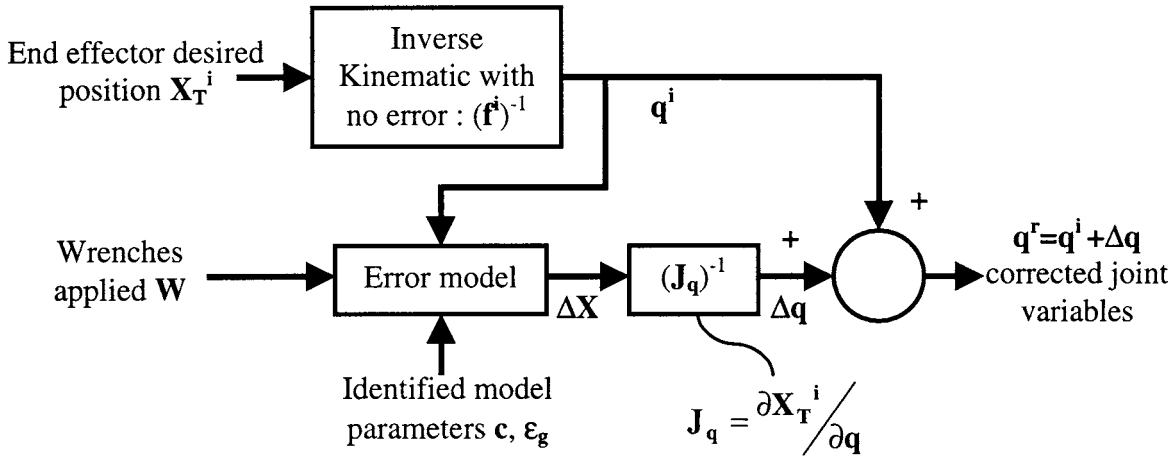

Fig. 3. Compensation algorithm.

3. MODEL PARAMETERS IDENTIFICATION

3.1. Parameters identification general principle

Equation (17) shows that only $\mathbf{M_e}$ depends on **W**. Therefore, at a given configuration **q**, if only the weight **W** varies, only the elastic errors will vary. Elastic errors can then be identified. Knowing the elastic errors, the geometric errors can be deduced.

Compliance parameters identification. The basic equation leading to the compliance parameters identification is obtained by the difference between Equation (17), with some weight **W**, and Equation (17), with some other weight $\mathbf{W_0}$. The equation is the following:

$$\mathbf{D\Delta X(q, W) = DM_e(q, W)c(q)} \tag{18}$$

With $\mathbf{D\Delta X(q, W) = \Delta X(q, W) - \Delta X(q, W_0)}$ and $\mathbf{DM_e(q, W) = M_e(q, W) - M_e(q, W_0)}$.

The left hand side of Equation (18) is the difference between measured errors at the weight pair **W** and $\mathbf{W_0}$ and at a given configuration **q**. The matrices $\mathbf{M_e(q, W)}$ and $\mathbf{M_e(q, W_0)}$ are calculated from there explicit forms.

When rotary joints are involved, **c** is independent of configuration. So any single rotary joint configuration may be used for the system construction. For prismatic joints, the compliance parameters for the i^{th} link are function only of q_i. Therefore, measuring each prismatic joint independently from the other joints is sufficient to identify the compliance parameters. For each link, the idea is to separate the constant and the variable parts of the corresponding vector $\mathbf{c_i}$. We have for the i^{th} link:

$$\mathbf{c_i}(q_i) = \Delta\mathbf{c_i}(q_i) + \mathbf{c_i}(0) \tag{19}$$

We call $\mathbf{q_i}$ the configuration where all joint variables but q_i are equal to zero, $\mathbf{q = 0}$ is called home configuration. Considering Equation (19), at $\mathbf{q_i}$, Equation (18) becomes:

$$\mathbf{D\Delta X(q_i, W) = DM_e(q_i, W)c(0) + DM_{ei}(q, W)\Delta c_i}(q_i) \tag{20}$$

Where $\mathbf{DM_{ei}(q, W) = M_{ei}(q, W) - M_{ei}(q, W_0)}$ and $\mathbf{M_{ei} = \partial\Delta X_e / \partial c_i}$.

Equation (19) shows that $\mathbf{c(0)}$ must first be determined followed by $\mathbf{\Delta c_i}$ at any q_i.

Geometric errors identification. Assuming that compliance parameters are known, Equation (17) can be written as follows:

$$\mathbf{\Delta X(q, W) - M_e(q, W)c = J(q)\varepsilon_g} \tag{21}$$

Where error $\mathbf{\Delta X}$ is measured and the product $\mathbf{M_e(q, W)c}$ as well as $\mathbf{J(q)}$ are solely calculated.

The vector $\boldsymbol{\varepsilon_{gi}}$ depends only on q_i, so, measuring errors while only joint i moves makes only $\boldsymbol{\varepsilon_{gi}}$ vary in Equation (21), the other $\boldsymbol{\varepsilon_{gi}}$ ($j \neq i$) keep their initial value (defined at home configuration, $\mathbf{q = 0}$). As for compliance parameters, the constant and the variable parts are separated:

$$\varepsilon_{gi}(q_i) = \Delta\varepsilon_{gi}(q_i) + \varepsilon_{gi}(0) \tag{22}$$

At $\mathbf{q_i}$, Equation (21) becomes:

$$\mathbf{\Delta X(q_i, W) - M_e(q_i, W)c(q_i) = J(q_i)\varepsilon_g(0) + J_i(q_i)\,\Delta\varepsilon_{gi}}(q_i) \tag{23}$$

Where $\mathbf{J_i}$ is equal to $\partial\mathbf{f}^r/\partial\boldsymbol{\varepsilon_{gi}}$. Equation (23) shows that $\boldsymbol{\varepsilon_g(0)}$ must first be determined followed by $\mathbf{\Delta\varepsilon_{gi}}$ at any q_i.

The algorithm of Figure 4 summarizes the parameters' identification general principle.

3.2. Parameters identification process

As stated above, the vectors $\mathbf{c(0)}$ and $\boldsymbol{\varepsilon_g(0)}$ must be evaluated before beginning the process shown in Figure 4.

The size of the vector **c** is generally higher than the number of equations in Equation (20). A system involving several weight pairs must then be built. We call b_0 the number of pairs. By definition, $\mathbf{\Delta c_i}$ is equal to zero at home. The system is written as follows:

$$\mathbf{D\Delta X^s = DM_e^s(q_i, W)c(0)} \tag{24}$$

In general, the System (24) has an infinite number of solutions. One solution, called $\mathbf{c^c(0)}$, is chosen, setting the redundant parameters equal to zero. No relation can be defined for $\boldsymbol{\varepsilon_g(0)}$, this vector is thus chosen equal to zero.

As it can be understood, the chosen solutions may not necessarily be the solutions which correspond to the physics of the considered manipulator. They are however used as inputs into the computation process. The parameters obtained are called $\mathbf{c^c(q)}$ and $\boldsymbol{\varepsilon_g^c(q)}$.

If we now consider the error measured, $\mathbf{\Delta X}$, and the error predicted, $\mathbf{\Delta X^c}$, by the model at (**q**, **W**), using $\mathbf{c^c}$ and $\boldsymbol{\varepsilon_g^c}$, the

https://doi.org/10.1017/S0263574702004058 Published online by Cambridge University Press

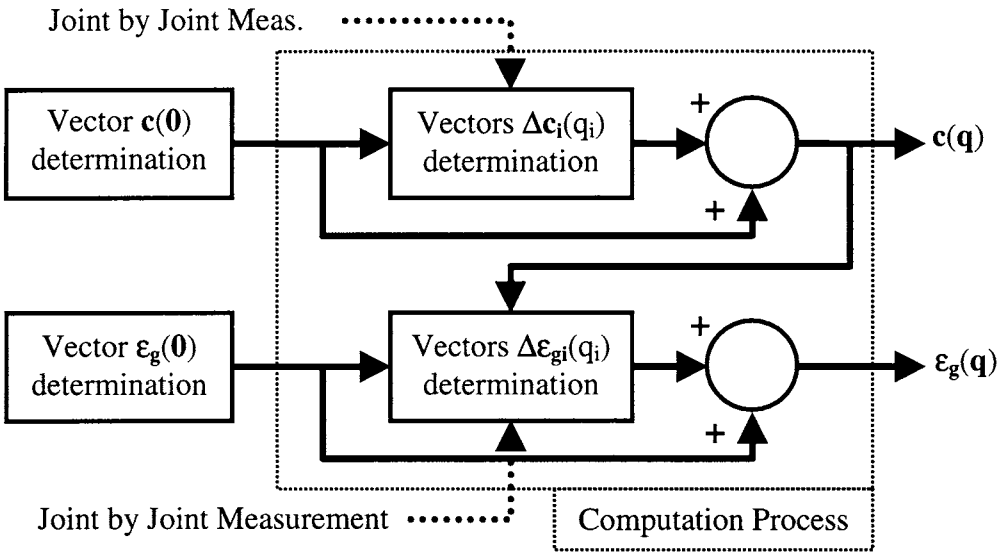

Fig. 4. Parameter identification algorithm structure.

predicted error may be different from the measured one. The Figure 5 shows how to identify parameters for an exact prediction of the errors.

In the following it is shown that the difference between $\mathbf{\Delta X}$ and $\mathbf{\Delta X^c}$ can be obtained in an explicit algebraic form. This difference may be equal to zero. In such a case, the choice $\mathbf{c^c(0)}$ and $\boldsymbol{\varepsilon}_g(\mathbf{0})=\mathbf{0}$ previously made, gives an exact prediction of the end-point errors. The identification process is then finished. If the difference is not equal to zero, see flag 1 of Figure 5. It will be shown that the difference always depend only of $\mathbf{c(0)}$ and $\boldsymbol{\varepsilon}_g(\mathbf{0})$ as it can be seen in the next expression:

$$\mathbf{\Delta X(q, W) - X^c(q, W) = M_c(q, W)c(0) + M_g(q)\varepsilon_g(0)} \quad (25)$$

Where matrices $\mathbf{M_c}$ and $\mathbf{M_g}$ are explicitly determined, where vector $\mathbf{\Delta X^c}$ is calculated with $\mathbf{c^c}$ and $\boldsymbol{\varepsilon}_g{}^c$ previously obtained and where vector $\mathbf{\Delta X}$ is measured.

The Equation (25) applied at several configurations gives some additional relations between the model parameters at home, see flag 2 of Figure 5. Then, new values will be chosen for $\mathbf{c(0)}$ and $\boldsymbol{\varepsilon}_g(\mathbf{0})$, see flag 3 of Figure 5. Implemented into the process body, these values insure the identification of correct model parameters. That is to say parameters which permit the right prediction of the errors without any additional work, see flag 4 of Figure 5.

The advantage of this process is that it is non-iterative, so no convergence problem can occur and a solution always exists.

4. APPLICATION TO THE PATIENT POSITIONER SYSTEM

4.1. Description, associated model, errors measurement technique, measurements to perform the identification process

Description. The PPS of the Northeast Proton Therapy Center (NPTC) at MGH is shown in Figure 6. A nozzle delivers a proton beam to the patient. The nozzle is carried by a large rotating gantry. The patient is carried by the end effector of the PPS manipulator[1,2,24]

The gantry rotation changes the angle of the beam. The point of intersection between the gantry axis of rotation and the beam is called the "isocenter". The PPS has to place the patient inside the gantry so that the tumor and the isocenter are coincident. The maximum acceptable radial error between the nominal tumor position and the isocenter is

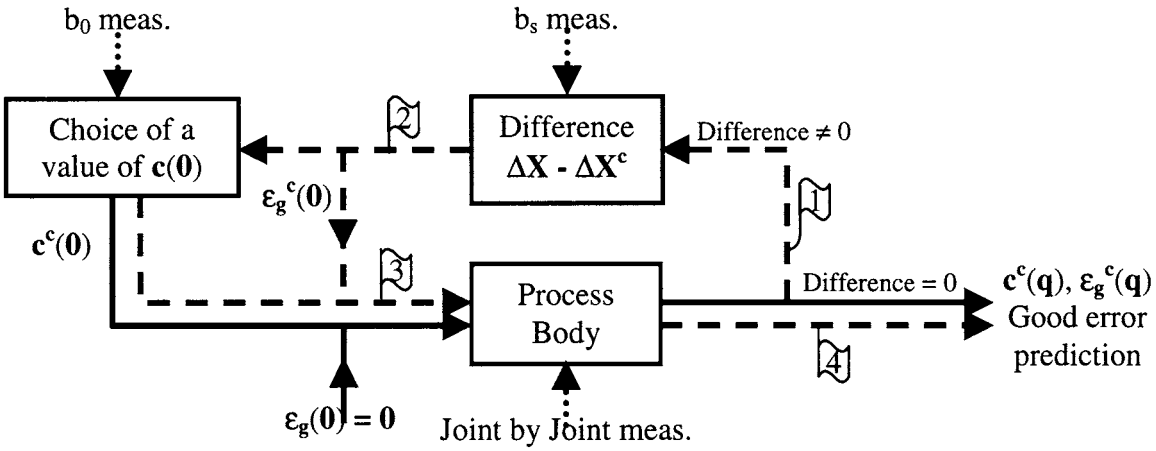

Fig. 5. Parameters identification process.

https://doi.org/10.1017/S0263574702004058 Published online by Cambridge University Press

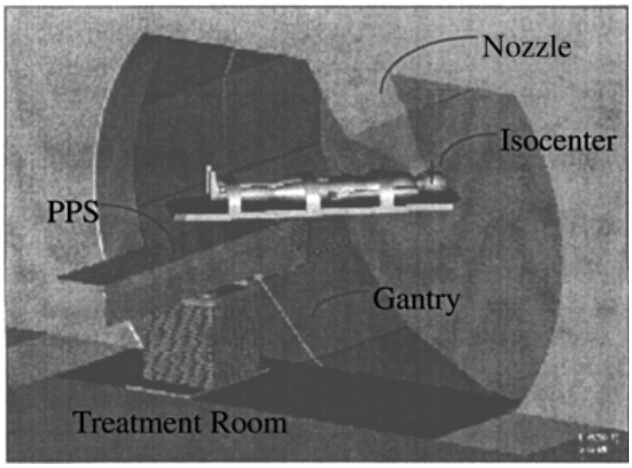

Fig. 6. NPTC patient positioner system.

0.5 mm since larger errors may result in the destruction of healthy tissues. Tests have shown that the PPS can not achieve this accuracy without error compensation algorithms. The inherent accuracy of the PPS is 7 mm because of its large cantilever design.

The PPS is shown in more detail in Figure 7. It is a six d.o.f manipulator designed by General Atomics, San Diego, CA. The first three joints are prismatic. The maximum travel of these joints is 225 cm for the lateral axis (X), 56 cm for the vertical axis (Y) and 147 cm for the longitudinal axis (Z). The last three joints are rotary joints. The first rotary joint has an axis of rotation parallel to the vertical axis (Y) and can rotate ±90 deg. The last two joints are used for small corrections around an axis of rotation parallel to the Z (roll) and X (pitch) axes, and have a maximum rotation angle of ±3 deg. The manipulator "end-point" is a couch which supports the patient in a supine position. The design accommodates supine patients up to 188 cm in height and up to 200 kg in weight in normal operations. The couch treatment volume is defined by a treatment area on the couch of 50 cm × 50 cm and a height of 40 cm.

The reference frames are shown in Figure 7. The inertial frame F_1 and the frame F_0 are similar and fixed at the base of the system. The frame F_1 moves with the first prismatic joint along the X direction, and is aligned with F_0 at the home position (position where all the joint variables are equal to zero). The frame F_2 moves with the top of the second linear joint in the Y direction. The frame F_3 moves with the end of the arm in the Z direction. F_4 rotates around the vertical axis of the frame F_3. F_6 is the reference system defined at the couch top O_T The point P_T is the treatment point such as the tumor in the patient's body. The point P_{TN} defines the center of the treatment volume and is called the nominal treatment point. A detail of the treatment area is shown in Figures 6 and 8.

The payload (patient, health care equipment and couch) wrench is measured by a 6 axis force/torque sensor placed between the couch and the last joint. This sensor gives the patient weight w_p and its center of gravity position on the couch (x_p, z_p).

Model of the PPS. Since the PPS is a 6 degrees of Freedom manipulator and the frames F_1 and F_0 are coincident, 36 geometric error parameters have to be considered in the model. The number of compliance parameters are reduced to 11 due to the PPS physics and loading. For instance, the base plate can be considered as rigid so that no compliance parameter is required here. Also, since the PPS loading is only due to gravity, and since the range of motion of the pitch and roll axis is very small, the wrench applied to each link has the form: $\mathbf{W} = [\,0\, F_y\, 0\, M_x\, 0\, M_z\,]$. The compliance

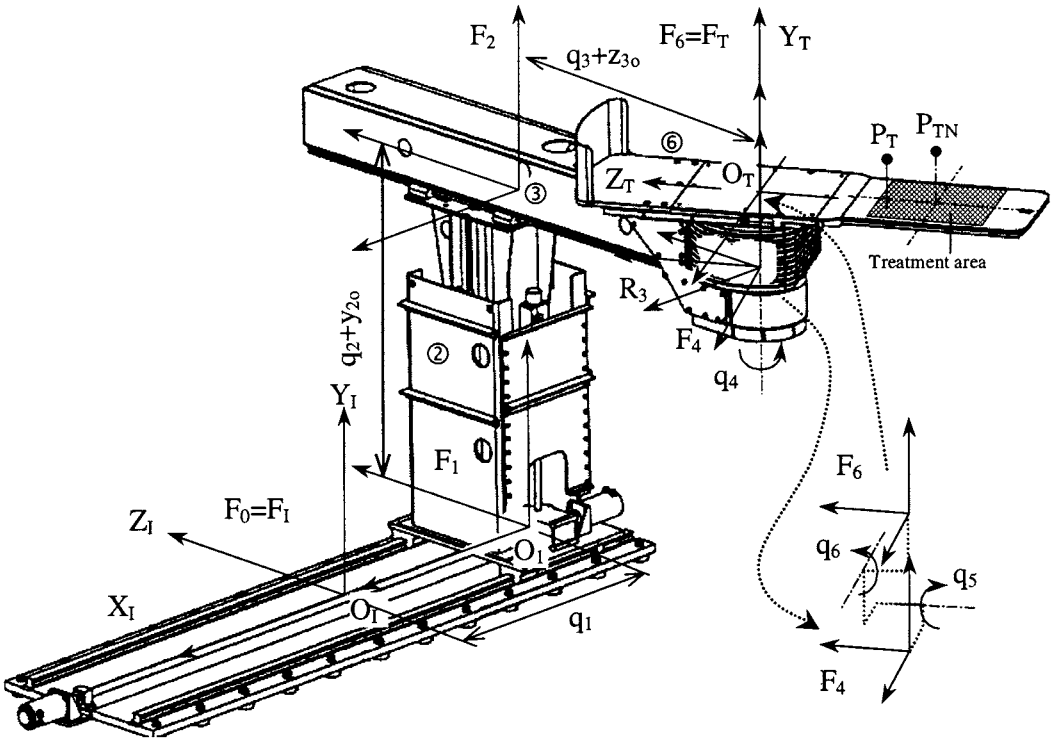

Fig. 7. Close view of the PPS and its reference frames.

https://doi.org/10.1017/S0263574702004058 Published online by Cambridge University Press

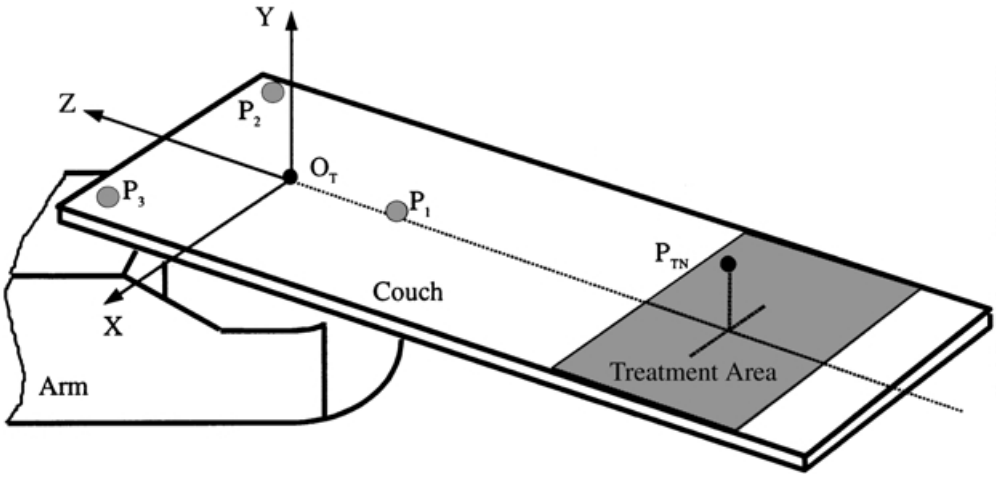

Fig. 8. Measurement points (P_1, P_2, P_3), nominal treatment point and O_T.

parameters multiplied by the nullified components of **W** in Equation (16) don't influence the elastic errors and hence don't need to be considered in the model. The compliance parameters of the second and third links are the only variable ones.

Error measurement technique. The errors of the PPS are measured using a Leica's 3D Laser Tracking System. Three cat-eye laser targets are mounted on the top of the couch in a triangle configuration around the vertical rotary axis 10 mm above the couch, see Figure 8. The center of the triangle $P_1P_2P_3$ is considered as the PPS end-point, O_T. The end effector frame Y_T is the vector perpendicular to the ($P_1 P_2 P_3$) plane. Axis X_T is the direction of the vector P_2P_3, and Z_T axis is the cross product of X_T and Y_T The errors are obtained by subtracting the measured frame position and orientation from their ideal values. The accuracy of the PPS position measurements at the 3D measurement points is estimated to be 0.04 mm.

Measurements to perform the identification process. The configurations and loading shown in Figure 9 are used for the **c**(**0**) identification, they are called initial configurations and loading. Note that, as compliance parameters associated with rotary joints are constant, configurations with q_4 different from zero can be used for the **c**(**0**) identification. Nine measurements per configuration and loading case are performed, leading to 63 measurements for **c**(**0**) identification.

For the identification of all the model parameters at any configuration, on the overall range of motion of joint 1, a resolution of 53 configurations have been chosen, 17 for joint 2, 31 for joints 3 and 4 and 19 for joints 5 and 6. The loading cases are the same as the ones described in Figure 9. This finally leads to 606 measurements in addition to the previous 63 ones.

4.2. Simulation results, error compensation accuracy dependency with repeatability

The behavior of the PPS is simulated using the generalized errors model given by Equation (13). The generalized errors vector has the following form:

$$\boldsymbol{\varepsilon} = \boldsymbol{\varepsilon}_g + \boldsymbol{\varepsilon}_e + \boldsymbol{\varepsilon}_r \tag{26}$$

The vector $\boldsymbol{\varepsilon}_g$ represents the geometric errors, they are simulated using simple mathematical functions such as sin function for straightness errors. The vector $\boldsymbol{\varepsilon}_e$ represents the elastic errors which are simulated using the beams theory. The vector $\boldsymbol{\varepsilon}_r$ takes in account all the random error aspects such as the resolution of the encoders.

The measurement of one point of the couch is simulated using the following expression:

$$\mathbf{X} = \mathbf{X}^i + \boldsymbol{\Delta}\mathbf{X} + \text{measurement errors}$$

The vector **X** is the simulated position of the considered point, $\mathbf{X}^i$ its ideal position without any error and $\boldsymbol{\Delta}\mathbf{X}$ the errors obtained with the generalized errors model.

In such conditions, the amplitude of the simulated errors at the nominal treatment point reaches about 10 mm when the PPS workspace is scanned.

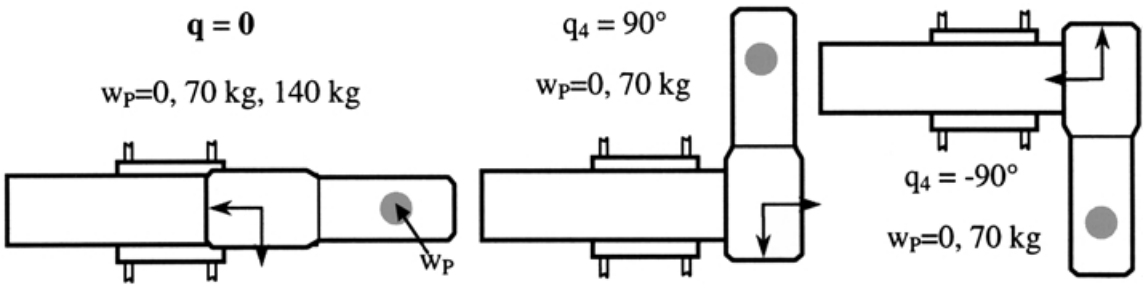

Fig. 9. Measurements initial configurations and loading.

https://doi.org/10.1017/S0263574702004058 Published online by Cambridge University Press

The simulated PPS repeatability is determined at the nominal treatment point. It is obtained from about 300 simulated measurements at random configurations and loads. The value of the repeatability can be modified by making the amplitude of $\boldsymbol{\varepsilon}_r$ vary [see Equation (26)].

The measurement of a set of 110 independent treatment configurations was simulated to verify the accuracy of the correction algorithm. The parameter identification computation, implemented in Matlab, required less than 30 minutes on a standard computer.

With a repeatability of 0.15 mm, which is supposed to be the case of the real system, the efficiency of the correction algorithm is excellent since more than 95% of the errors are compensated. The Figure 10 shows the initial errors without correction, as small circles, and remaining errors after compensation, called residual errors, as crosses. Thanks to the 0.5 mm radius circle, we see that the residual errors are under the PPS accuracy specification limit. Figure 11 shows the statistical distribution of the residual errors and permits us to estimate their value at 0.41 mm.

If we now make the repeatability value change, Figure 12 shows that the efficiency of the correction algorithm closely depends on this value. We see that if the repeatability stays under 0.2 mm, the PPS accuracy specification of 0.5 mm is met.

Note that even if the error compensation accuracy is higher than the PPS specification for repeatability values higher than 0.2, the results are still very good compared to the problem difficulty.

4.3. Error compensation in site results, reduction of the measurement requirements

A total of 270 measurements were performed at the Nominal Treatment Point (P_{TN}). Figure 13 shows the error distribution for each axis. From these measurements, the

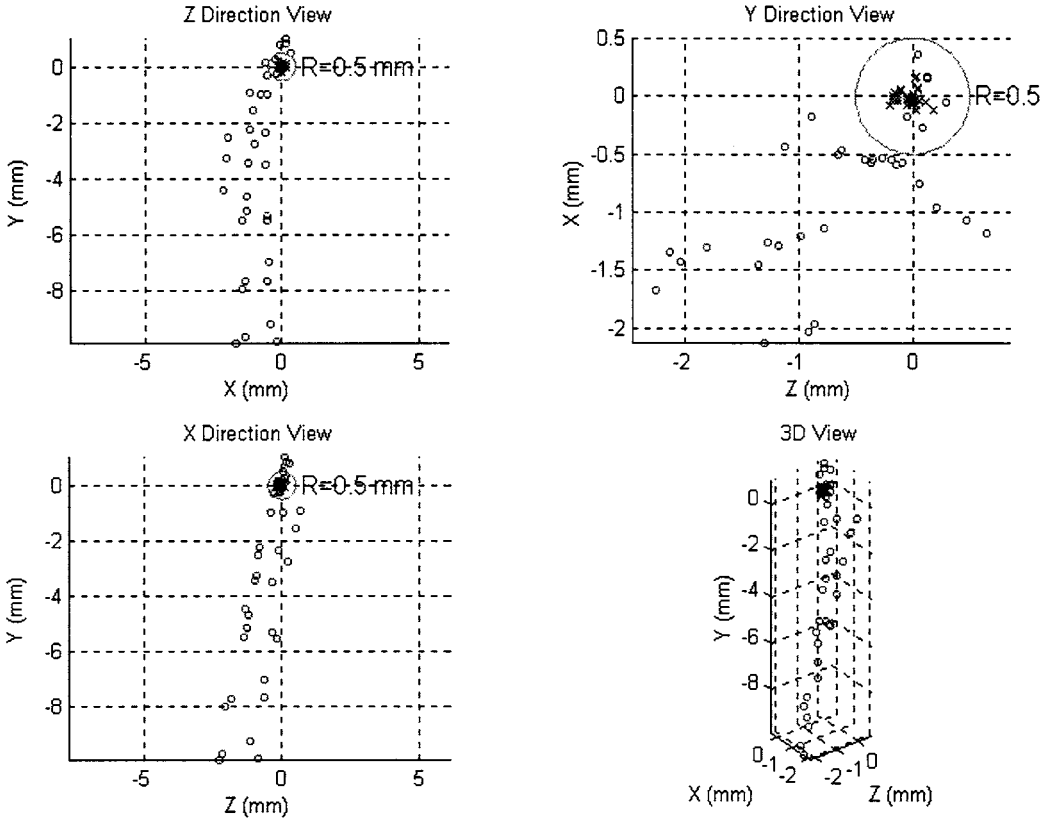

Fig. 10. Graphical representation of initial and residual errors at P_{TN}.

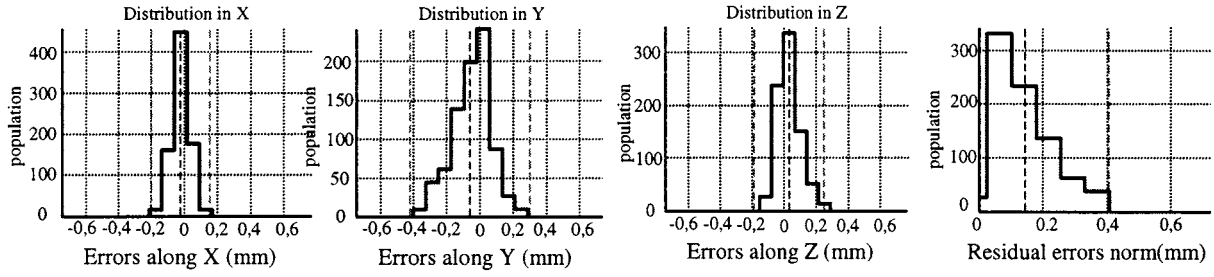

Fig. 11. Statistical distribution of residual errors at P_{TN}.

https://doi.org/10.1017/S0263574702004058 Published online by Cambridge University Press

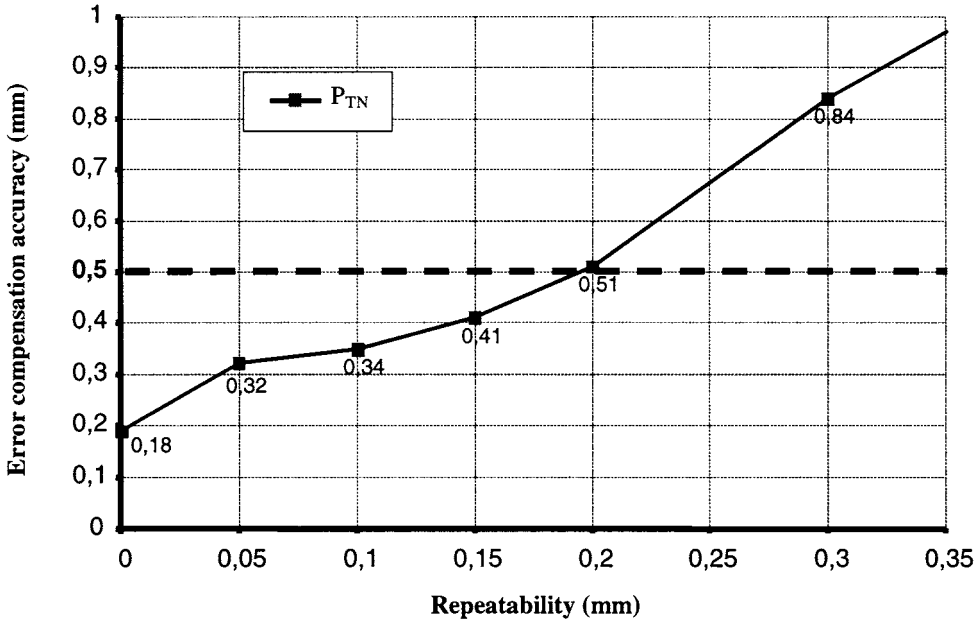

Fig. 12. Error compensation accuracy with respect to PPS repeatability.

repeatability of the PPS system in site is estimated to be 0.14 mm which is very close to the simulated value.

The measured and uncompensated error amplitude in the system reaches an 8 mm range which is a slightly less than what was simulated. Hence the assumption that the errors are small compared to the size of the system is satisfied. Furthermore, since the system is stationary during treatment, the quasi-static assumption is also satisfied. The linearity of the elastic deformations with respect to the load has also been verified. The nonlinear effects of **W** were measured to be under 0.041 mm for a payload on the couch varying from 0.0 to 150.0 kg.

In addition to the 669 measurements used for the parameters' identification, a set of 110 independent treatment configurations were measured to verify the accuracy of the correction algorithm.

Figure 14 shows the statistical distribution of the residual errors that are not compensated for by the correction algorithm. Clearly, it shows that 98.6% of the residual errors at P_{TN} are under 0.45 mm and that the compensation

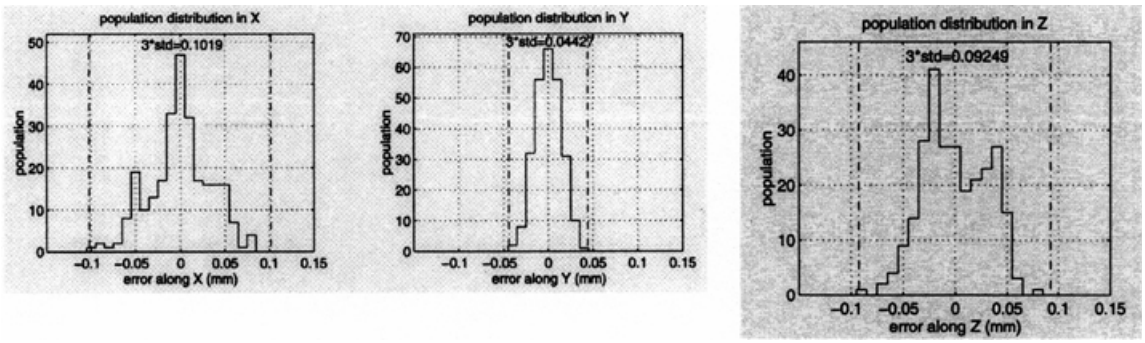

Fig. 13. Repeatability statistical results.

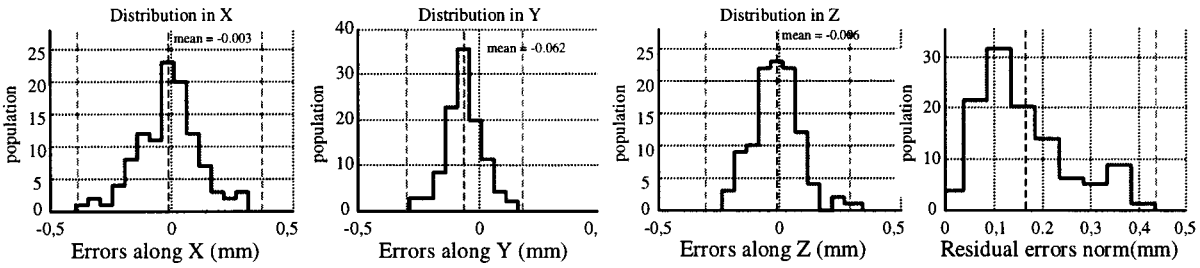

Fig. 14. Statistical distribution of the residual P_{TN} errors.

https://doi.org/10.1017/S0263574702004058 Published online by Cambridge University Press

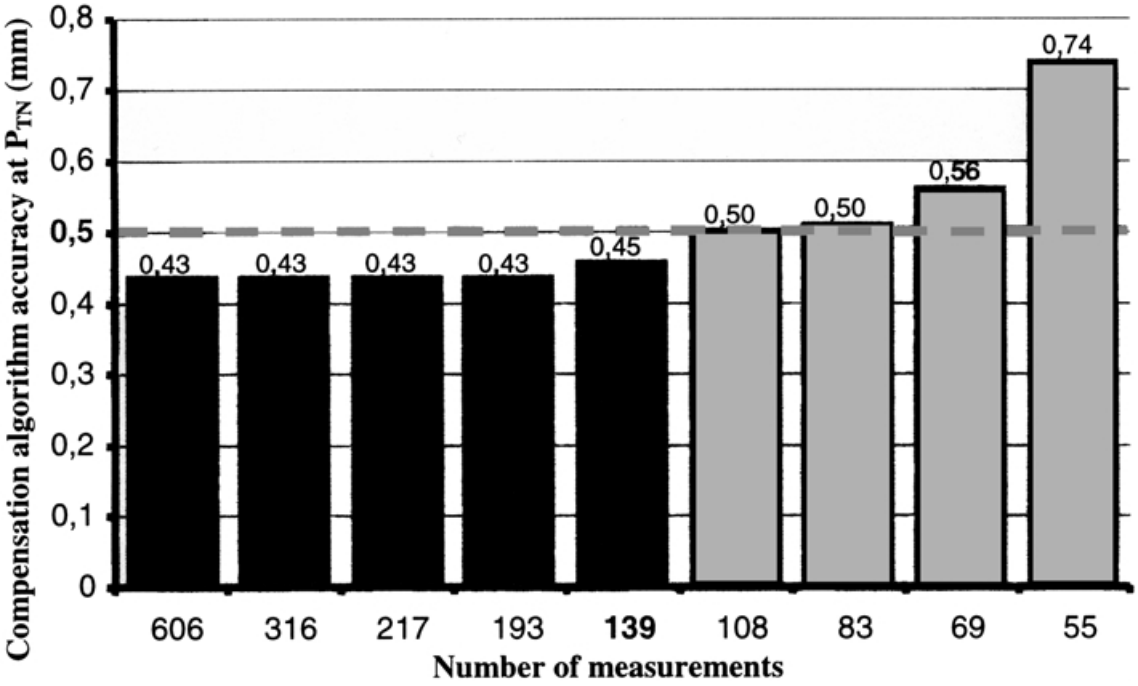

Fig. 15. Compensation accuracy evolution with the number of measurements.

algorithm reduces the errors by approximately a factor of 20, which enables the PPS to meet its specifications.

We considered that it was possible to reduce the number of measurements needed to identify the parameters, at any configuration. This was verified. Figure 15 shows that, to achieve the precision requirements for our application, the number of measurements could be reduced to as low as 139 measurements instead of 606. So only a total of 202 measurements are needed to identify all the model parameters.

5. CONCLUSION

In this paper, a method to compensate for the geometric and elastic errors is developed. In the method, a model of the end-point errors of the system is developed in terms of geometric and compliance parameters. These are identified off-line using experimental measurements. The models then are used to correct for errors during system operation. The method is applied to the new high accuracy medical manipulator, called the Patient Positioner System. The simulation results show that a very good error compensation accuracy can be obtained and that this accuracy depends on the repeatability of the PPS. The experimental results coincide very closely with the simulation enabling this system to meet its design specifications. The method is relatively simple, inexpensive and requires a small computational effort. It does not require any measurements during system operation and needs only a relatively low number of measurements for the parameters' identification.

ACKNOWLEDGMENTS

The support for this work by the University of Poitiers "Laboratoire de Mécanique des Solides", the Northeast Proton Therapy Center from the Massachusetts General Hospital and the PPS technical information provided by General Atomics, San Diego, CA, are acknowledged and appreciated.

References

1. J. Flanz et al., "Overview of the MGH-Northeast Proton Therapy Center plans and progress," *Nuclear Instruments and Methods in Physics Research B* **99**, 830–834 (1995).
2. J. Flanz et al., "Design Approach for a Highly Accurate Patient Positioning System for NPTC," *Proceedings of the PTOOG XXV and Hadrontherapy Symposium*, Belgium (September, 1996) pp. 1–5.
3. C. Mavroidis, J. Flanz, S. Dubowsky, P. Drouet and M. Goitein, "High Performance Medical Robot Requirements and Accuracy Analysis", *Robotics and Computer Integrated Manufacturing* **14**, No. 5–6, 329–338 (Dec., 1998).
4. C. Mavroidis, S. Dubowsky, P. Drouet, J. Hintersteiner and J. Flanz, "A Systematic Error Analysis of Robotic Manipulators: Application to a High Performance Medical Robot," *Proceedings of the 1997 International Conference in Robotics and Automation*, Albuquerque, NM (April, 1997) pp. 980–985.
5. M.A. Meggiolaro, C. Mavroidis and S. Dubowsky, "Identification and Comparison of Geometric and Elastic Errors in Large Manipulators: Application to a High Accuracy Medical Robot." *Proceedings of the 1998 ASME Design Engineering Technical Conferences*, Atlanta, GA (September, 1998) Paper No. DETC98/MECH-5947.
6. Z.S. Roth, B. Mooring and B. Ravani, "An Overview of Robot Calibration," *IEEE Journal of Robotics and Automation* **RA-3**, No. 5, 377–385 (Oct., 1987).
7. E. Dombre and W. Khalil, *Modélisation et Commande des Robots* (Hermes, 1988).
8. B. Gorla and M. Renaud, *Modèles des Robots Manipulateurs* (Cépadues Editions, 1984).
9. C. Mirman and K. Gupta, "Robot Parameter Identification and Compensation Using Sets of Jacobian Matrices," *Eighth World Congress on the Theory of Machines and Mechanisms*, Prague, Czechoslovakia (August 26–31, 1991) pp. 483–486.
10. H. Zhuang and L.K. Wang and Z.S. Roth, "Error-Model-Based Robot Calibration Using a Modified CPC Model," *Robotics & Computer Integrated Manufacturing* **10**, No. 4, 287–299 (1993).

https://doi.org/10.1017/S0263574702004058 Published online by Cambridge University Press

11. P. Broderick and R. Cirpa, "A Method for Determining and Correcting Robot Position and Orientation Errors Due to Manufacturing," *Transactions of the ASME, Journal of Mechanisms Transmissions and Automation in Design* **110**, 3–10 (1988).
12. L. Everett and J. Lei, "Improved Manipulator Performance Through Local D-H Calibration," *J. Robotics Systems* **12**, No. 7, 505–514 (1995).
13. J. Hollerbach and C. Wampler, "The Calibration Index and Taxonomy for Robot Kinematic Calibration Methods," *Int. J. Robotics Research* **15**, No. 6, 573–591 (Dec., 1996).
14. L. Everett and T. Ives, "A Sensor Used for Measurements in the Calibration of Production Robots," *Proc. IEEE int. Conf. In Robotics and Automation* (1993) pp. 174–179.
15. M. Vincze, J.P. Prenninger and H. Gander, "A Laser Tracking System to Measure Position and Orientation of Robot End Effectors Under Motion," *Int. J. Robotics Research* **13**, No. 4, 305–314 (August, 1994).
16. H. Zhuang, Z.S. Roth and K. Wang, "Robot Calibration by Mobile Camera Systems," *J. Robotic Systems* **11**(3), 155–167 (1994).
17. J. Borm and C. Menq, "Determination of Optimal Measurment Configurations for Robot Calibration Based on Observability Measure," *Int. J. Robotics Research* **10**, No. 1, 51–63 (Feb., 1991).
18. H. Zhuang, J. Wu and W. Huang, "Optimal Planning of Robot Calibration Experiments by Genetic Algorithms," *Proceedings of the 1996 IEEE International Conference on Robotics and Automation*, Mineapolis, Minnesota (April, 1996) **Vol. 2**, pp. 981–986.
19. L. Everett and J. Lei, "Improved Manipulator Performance Through Local D-H Calibration ," *J. Robotics System* **12**, No. 7, 505–514 (1995).
20. W.S. Sunada and S. Dubowsky, "On the Dynamic Analysis and Behavior of Industrial Robotic Manipulators with Elastic Members," *J. Mechanical Design, Transactions of the ASME* **105**, No. 1, 42–51 (March, 1983).
21. D.E. Whitney, C.A. Lozinski and J.M. Rourke, "Industrial Robot Forward Calibration Method and Results," *J. Dynamics Systems, Measurement, and Control* **108**, 1–8 (March, 1983).
22. J. Craig, *Introduction to Robotics: Mechanics and Control* (Addison Wesley, 1989).
23. L. Chevalier, *Mécanique des systèmes et des milieux déformables* (édition . Ellipse France, 1996).
24. J. Flanz, "Large Medical Gantries." *Proceedings of the 1995 Particle Accelerator Conference*, (April, 1995) pp. 2004–2008.

https://doi.org/10.1017/S0263574702004058 Published online by Cambridge University Press